

research direction. This necessitates efforts towards designing more flexible and scalable deep learning models, enhancing representational and learning methodologies for models, and developing efficient learning and reasoning algorithms. By surmounting these challenges, we can propel the application and advancement of deep learning in graphical reasoning problems, providing smarter and more efficient solutions for a myriad of practical problems.

For instance, problems like Ravens Progressive Matrices (RPM) [15] and Bongard problems [16], [17] present learning requirements that span from perception to reasoning.

A. The RAVEN database

The RAVEN database [18], a subset of the broader RPM (Raven’s Progressive Matrices) problem set, typically comprises of 16 geometric entity-based images. These are structured into a problem statement consisting of 8 images and an answer pool containing the remaining 8 images. The objective for subjects engaging with this database is to select the appropriate images from the answer pool, enabling the completion of a 3x3 matrix within the problem statement. This matrix construction challenges individuals to discern specific abstract concepts embodied by the progressive patterns of geometric images arranged in a row-wise manner.

As exemplified in figure1, the construction of RAVEN problems adheres to a structured framework. Within this framework, human-defined concepts inherent to geometric images, such as "shape" and "color", undergo a process of artificial abstraction. This abstraction transforms these concepts into bounded, countable, and precise "visual attribute" values. Subsequently, the notion of "rule" is invoked to delineate the systematic progression of a circumscribed set of "visual attribute" values. It is noteworthy that certain visual attributes remain unconstrained by the "rule", potentially introducing elements of interference in the reasoning processes of deep models.

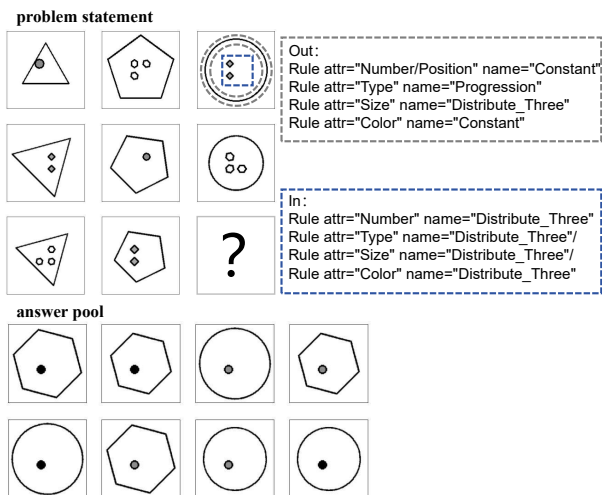


Fig. 1. RAVEN case

The generative process for a complete RAVEN problem commences with the selection of a rule sample from a prede-

efined rule repository. This is followed by the design of visual attribute values aligned with the contents of the chosen "rule". Attributes not governed by the rule undergo random value assignments. Subsequently, image rendering occurs based on the generated "attribute" information.

The RAVEN database exhibits diversity through its multiple sub-databases. These include single-rule groups: center single (center), distribute four ($G2 \times 2$), distribute nine ($G3 \times 3$), and double-rule groups: in center single out center single (O-IC), up center single down center single (U-D), left center single right center single (L-R), in distribute four out center single (O-IG). In problems adhering to single-rule variations, the progressive attribute changes within image entities are bound by a unitary set of rules. Conversely, double-rule variations enforce constraints via two independent sets of rules, augmenting the complexity of the problem.

B. Pgm database

Pgm [19] and RAVEN problems exhibit a striking parallelism in their design philosophy, with both frameworks employing a problem statement consisting of 8 images and an answer pool supplemented by an additional 8 images. A unique facet of PGM problems is the expansion of the "rule" concept, which not only encompasses the progressive patterning of "visual attributes" horizontally within the matrix but also vertically. An illustrative example of a PGM problem is presented in the accompanying figure 2, highlighting its intricate nature.

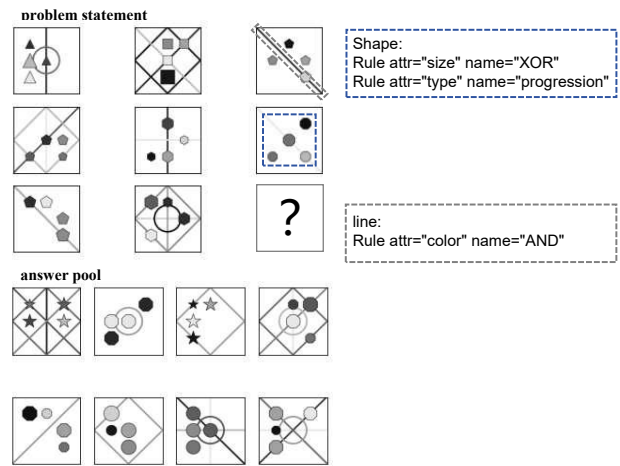


Fig. 2. PGM case

The intricacy of RPM problems, therefore, arises not only from the extraction of visual attributes across multiple hierarchies but also from the challenge of inducing and learning the progressive patterns displayed by these "visual attributes." This emphasizes the significance of discerning not only the attributes themselves but also their structural progression within these problems, a task that requires a nuanced understanding of both the individual components and their interrelationships within the problem context.

C. Bongard-logo database

Bongard problems [16], contrasting with RPM (Raven’s Progressive Matrices) problems, are noteworthy exemplars of small-sample learning challenges. These problems typically present a series of images divided into two distinct groups: primary and auxiliary. The primary group comprises images that adhere to a specific set of rules defining an abstract concept, whereas the auxiliary group includes images that deviate from these rules in varying degrees. The intricacy of Bongard problems lies in the requirement for deep learning algorithms to precisely categorize ungrouped images into their corresponding groups based on subtle pattern recognition and abstract reasoning.

Within the domain of abstract reasoning, Bongard-logo [17] problems serve as a particular instantiation of Bongard problems, posing a significantly high level of reasoning difficulty. Each Bongard-logo problem consists of 14 images, with 6 images belonging to the primary group, 6 to the auxiliary group, and the remaining 2 serving as categorization options. These images are comprised of various geometric shapes, and the arrangements of these shapes serve as the basis for grouping. Figure 3 illustrates an exemplary Bongard-logo problem, showcasing the complexity and abstract nature of these challenges.

In figure 3, each Bongard problem is comprised of two distinct image sets: primary group A and auxiliary group B. Group A contains 6 images, with the geometric entities within each image adhering to a specific set of rules. Conversely, group B includes 6 images that deviate from the rules established in group A. The task at hand requires determining whether the images in the test set align with the rules dictated by group A. The level of difficulty associated with these problems varies depending on their structural complexity.

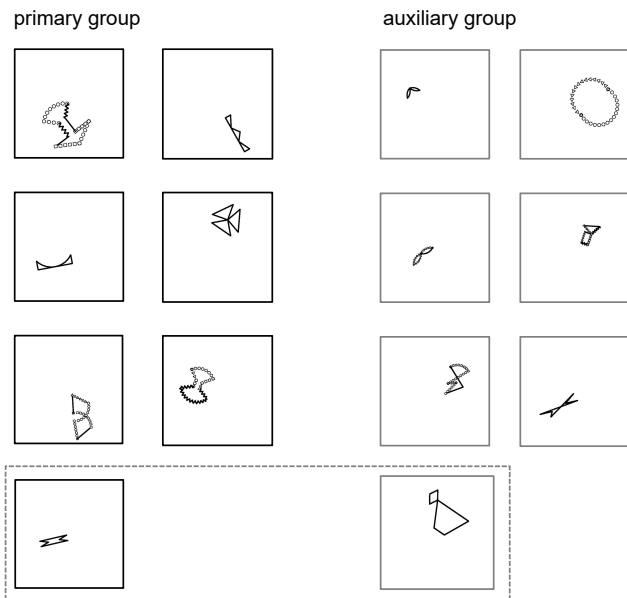


Fig. 3. Bongard case

Furthermore, Bongard-logo problems are classified into three distinct conceptual categories: 1) Free Form problems

(ff), in which each shape is composed of randomly sampled action strokes, potentially resulting in one or two shapes per image; 2) Basic Shape problems (ba), corresponding to the identification of a single shape category or combinations of two shape categories represented within given shape patterns; and 3) Abstract Concepts (hd), designed to assess a model’s proficiency in discovering and reasoning about abstract concepts such as convexity, concavity, and symmetry. These categorizations underscore the breadth and depth of reasoning abilities required to tackle Bongard-logo problems effectively.

II. RELATED WORK

This section is devoted to comprehensively presenting the significant research achievements related to the RPM (Raven’s Progressive Matrices) problem and the Bongard-Logo problem, as derived from past studies. These notable research milestones have played a pivotal role in driving forward the advancements in the field of artificial intelligence, specifically in relation to abstract reasoning capabilities. By thoroughly examining these milestones, we aim to foster a deeper understanding of the complexities and nuances associated with abstract reasoning challenges. Moreover, we hope to provide invaluable insights and guidance that can serve as a springboard for future research efforts, ultimately contributing to the continued growth and development of AI capabilities in tackling abstract reasoning tasks.

A. Graphical abstract reasoning dataset

The original RAVEN dataset [18] possessed a significant flaw in its candidate answer generation process. Specifically, each incorrect answer within the candidate set had only one erroneous visual attribute value, with the rest being identical to the correct answer. Consequently, the most frequent value among the candidate answers for each visual attribute would correspond to the correct visual attribute value. As a result, models could achieve remarkably high accuracy by merely considering the answer pool as input, without accounting for the question matrix’s statement section. This rendered the performance on the RAVEN database an inadequate reflection of the model’s true capabilities. To address this limitation, I-RAVEN [20] and RAVEN Fair [21] were developed as remedies.

In the realm of computer vision, the success of deep learning models often hinges on extensive data availability. However, the initial Bongard problems comprised only 100 instances, and even subsequent expansions left the question count relatively limited. Given that deep learning’s remarkable strides in computer vision are largely data-dependent, Nie et al. developed a procedurally generated technique to address the data scarcity issue, resulting in the Bongard-Logo [16] benchmark database for Bongard problems. This comprehensive database encompasses 2000 Bongard problems, categorized into three main types: free-form problems, basic-shape problems, and abstract-shape problems.

In free-form problems, the shape patterns within the test set exhibit longer strokes compared to those in the training set. The basic-shape problem test set poses challenges in

recognizing combinations of two shapes, with these foundational shapes appearing only once in the training set, ensuring no conceptual overlap between the test and training sets. The abstract-shape problem test set is further bifurcated: the combined abstract shape test set and the novel abstract shape test set [12]–[14].

Within the combined abstract shape test set, 20 pairwise combinations of two abstract attributes are randomly selected, with 20 problems per combination. While all individual attributes in this test set have been observed separately in the training set, these 20 novel combinations are exclusive to the test set. This necessitates the model’s ability to comprehend abstract shape concepts and utilize them in combinations. On the other hand, the novel abstract shape test set extracts one attribute from the training set along with all its combinations with other attributes. All questions related to the retained attribute are unique in this test set. The specialized test sets demand that models not merely memorize shape concepts but also demonstrate combinatorial generalization and extrapolation capabilities [12]–[14]. These rigorous test sets aim to evaluate the model’s profound understanding of shape concepts and its innovative prowess.

B. RPM solver

Discriminative models designed for image reasoning tasks typically output a multidimensional vector, in which each dimension corresponds to the likelihood of selecting a particular graph from a set of candidate answers as the correct response. These models vary in their approach to learning and inference.

The CoPINet model [22], for instance, introduces a novel contrast module that enables the network to learn subtle differences between input graphs. This is complemented by an inference module that distills potential underlying rules from the graph structures. By contrast, the LEN+teacher model [23] leverages a student-teacher paradigm to determine optimal training sequences and make predictions based on this guided learning.

The DCNet model [24] takes a different approach, employing a dual contrast module to directly compare rule rows and columns. This allows the model to pinpoint differences among candidate answers more precisely. Meanwhile, the NCD model [25] eschews traditional supervised learning methods, instead opting for an unsupervised approach that incorporates pseudo-targets and decentralization techniques to train the network.

In the context of subgraph-level analysis, SCL [26] establishes multiple monitors for subgraphs within reasoning problems. This ensures that each branch of the model can focus on specific visual attributes or rules, enhancing the model’s ability to handle complex reasoning tasks. SAVIR-T [27] further extends this concept by extracting information not only within subgraphs but also between them, providing a more holistic view of the reasoning problem and thus improving reasoning capabilities.

Recent research has also highlighted the benefits of using relatively decoupled perceptual visual features for reasoning tasks. These features, when combined with symbolic attention methods, offer not only higher reasoning accuracy but also

stronger model interpretability. This is exemplified in the PrAE [28] model, where neurosymbolic systems incorporate prior knowledge of rules to perform probabilistic reasoning and generate answer images.

On the other end of the spectrum, models like ALANS [29] eliminate the need for prior rule knowledge entirely. Despite this, they demonstrate superior generalization capabilities compared to end-to-end models. This underscores the importance of balancing learning and inference in complex reasoning tasks.

NVSA [30], employs holographic vectorized representations along with ground-truth attribute values to construct a neural-symbolic model, aiming to enhance the model’s comprehension and reasoning capabilities. This approach combines the strengths of both neural networks and symbolic logic, leveraging their respective advantages in handling continuous data patterns and discrete symbolic rules.

Finally, RS-CNN [31] and RS-TRAN [31] combine the best aspects of the aforementioned methods to achieve state-of-the-art results on RPM problems. RS-TRAN, in particular, leverages the powerful Transformer-Encoder architecture to tackle RPM problems from multiple perspectives and through multiple inferences. Meanwhile, RS-CNN adopts a multi-scale and multi-inference approach that combines both local and global information for more accurate reasoning [37]. In this paper, we have designed a novel standard layer that can replace the conventional Transformer-Encoder within RS-Tran. When this new layer is integrated, RS-Tran exhibits significant improvement in inference progress, demonstrating its enhanced efficiency and performance.

Overall, these models represent the cutting edge of image reasoning research and offer promising directions for future work.

C. Bongard solver

In recent years, three main approaches have been employed to address Bongard problems: methods based on language feature models, methods based on convolutional neural network models, and generated datasets.

Methods based on language feature models [16]: some researchers proposed a solution leveraging image-based formal languages, transforming image information into symbolic visual vocabulary, and subsequently tackling BP problems via symbolic languages and Bayesian inference. However, the limitation of this approach lies in its inability to directly apply to complex, abstract conceptual BP problems due to the need for reconstructing symbolic systems.

Methods based on convolutional neural network models [32]: some researchers constructed an image dataset consisting of simple shapes and utilized these images for pre-training to cultivate a feature extractor. Subsequently, image features from Bongard problems were extracted for image classification, determining whether test images conformed to the rules. Yun adopted a similar approach, initially pre-training with images containing visual features from BP problems to extract BP image features and then integrating an additional classifier for discrimination.

Methods based on Generated datasets [17]: some researchers employed fundamental CNNs, relation networks like WReN-Bongard, and meta-learning techniques, but their performance on the Bongard -Logo database was less than optimal.

These represent the main solutions targeted at Bongard problems in recent years, each with its own strengths and limitations.

D. Capsule Network

Capsule Networks (CapsNets) [33] are a novel deep neural network architecture. The design inspiration for this model comes from the “capsule” structures in the human brain, which are able to effectively process different types of visual stimuli and encode information such as position, shape, and speed.

In the context of deep learning, a capsule is a collection of embedded neurons, and a CapsNet is composed of capsules rather than individual neurons. It operates through a dynamic routing algorithm to update network weights, enabling the network to better understand and recognize features in images. Compared to traditional Convolutional Neural Networks (CNNs), CapsNets demonstrate stronger feature representation capabilities and improved performance.

Specifically, each capsule in a CapsNet represents a specific feature detector. The output of a capsule is a vector, where the length of the vector represents the probability of the feature’s existence, and the direction of the vector encodes the pose information of the feature. As a feature moves within the network, the output vector of the capsule changes accordingly, while maintaining its length (i.e., the probability of the feature’s existence).

Furthermore, CapsNets utilize an agreement-based dynamic routing algorithm as an alternative to the Max-Pooling operation in traditional CNNs. This dynamic routing algorithm can automatically adjust the structure and connection weights of the network based on the characteristics of the current input data, thereby enhancing the network’s performance and generalization capabilities.

The Capsule Network learns corresponding pose matrices for all local representations of an image, which are utilized to map these local representations onto high-dimensional representations within the object space. Through the Gaussian Routing algorithm, the Capsule Network computes the weights of these mapped high-dimensional representations. These weights are then applied to calculate a weighted sum of the high-dimensional representations, with the compressed summation result indicating pose consistency among local features within the image. During the training process, the pose matrices adapt to learn the relative positional relationships among local representations.

Currently, CapsNets are primarily applied in the field of image recognition and have demonstrated impressive performance on several benchmark tests.

E. Transformer

The Transformer [4] architecture is a distinctive deep learning framework that revolves around the self-attention mechanism to capture global dependencies within input sequences.

Comprising of an encoder and a decoder, both structured with stacked layers of multi-head self-attention and feed-forward neural networks, the Transformer offers a paradigm shift in sequential data processing.

Initially, the input sequence undergoes an embedding layer transformation into fixed-dimensional vectors, augmented with positional encoding to retain positional information within the sequence. Subsequently, the encoder, composed of multiple identical layers, each encompassing two sub-layers, commences its operation. The first sub-layer, the multi-head self-attention layer, calculates attention scores between different positions in the input sequence, capturing global dependencies. The second sub-layer comprises a simple fully connected feed-forward neural network. Both sub-layers are followed by layer normalization operations and residual connections, ensuring model stability and training efficiency.

The decoder section, also comprising multiple identical layers, introduces an additional encoder-decoder multi-head attention layer in each decoding layer. This attention layer enables the decoder to attend to the encoder’s output during the generation of the output sequence, facilitating interaction between the encoder and decoder. Furthermore, the self-attention layers in the decoder incorporate a masking mechanism to prevent consideration of future information when generating outputs for the current position.

The uniqueness of the Transformer architecture lies in its exclusive reliance on attention mechanisms, circumventing the inherent sequential computation limitations of traditional recurrent and convolutional neural networks. This design allows for parallel processing of input sequences, significantly enhancing training speed and model performance. Additionally, the Transformer exhibits impressive scalability, accommodating tasks of varying scales and complexities through the addition of encoder and decoder layers and adjustment of model parameters.

In summary, the Transformer architecture’s innovative approach to sequence modeling, characterized by its reliance on self-attention mechanisms and parallel processing capabilities, has ushered in a new era of advancements in natural language processing and beyond.

F. Vision Transformer

Vision Transformer (ViT) [34] is a groundbreaking image classification model that adapts the Transformer architecture from the domain of Natural Language Processing (NLP) and applies it successfully to Computer Vision (CV) tasks. The uniqueness of ViT lies in its treatment of images as sequential data, akin to text sequences in NLP, thereby leveraging the powerful sequence modeling capabilities of the Transformer.

In ViT, the input image is initially divided into fixed-size patches, which are then flattened and transformed into feature vectors through linear transformations. These feature vectors are augmented with positional encodings to retain their spatial positional information within the image. Subsequently, the processed feature vectors are fed into a standard Transformer encoder for processing.

The Transformer encoder comprises multiple layers of self-attention and feed-forward neural networks, arranged in a

stacked manner. The self-attention layers capture dependencies between different positions within the input sequence, while the feed-forward neural networks introduce non-linear transformations to enhance the model’s expressive power. Residual connections and layer normalization techniques are employed in each layer of the encoder to ensure model stability and convergence speed.

Ultimately, the output from the Transformer encoder is fed into a fully connected layer for classification, yielding the predicted categories for the image. Due to its sequence-to-sequence modeling approach similar to NLP, ViT effectively handles images of various sizes and resolutions and exhibits impressive scalability.

In summary, by adapting the Transformer architecture from NLP, Vision Transformer (ViT) has ushered in a new era of advancements in Computer Vision. Its emergence has not only challenged the dominance of traditional Convolutional Neural Networks (CNNs) in image classification tasks but has also laid a solid foundation for the development of subsequent visual Transformer models.

G. Sinkhorn distance

The Sinkhorn distance [35] is a notion derived from the field of optimal transport theory, offering a computationally efficient alternative to the classical Wasserstein distance [36]. At its core, it approximates the cost of transporting mass from one probability distribution to another by relaxing the constraint of mass preservation through a regularization term. This regularization, typically parameterized by a scalar value known as the entropy regularization parameter, allows for a smoother, more tractable optimization problem.

The Sinkhorn algorithm, closely associated with this distance, iteratively updates two sets of scaling factors until convergence to a solution that minimizes the regularized transport cost. This approach is particularly advantageous in high-dimensional settings or when dealing with large datasets, as it avoids the expensive linear programming computations required by the standard Wasserstein distance. The Sinkhorn distance offers a means to measure the similarity between two distributions solely based on samples drawn from them, without the need to have explicit knowledge of their underlying forms. This advantage sets it apart as a powerful tool in scenarios where direct access to the distributional forms is not feasible.

III. METHODOLOGY FOR BONGARD-LOGO

The Bongard-logo [16] and Raven’s Progressive Matrices (RPM) [15] tasks are both paradigms of abstract reasoning that necessitate the extractor’s adeptness in unveiling precise concepts veiled within abstract representations. These concepts are indicative of more elevated abstractions, surpassing rudimentary ideas such as “pixel configuration patterns”. Frequently, these elevated abstractions encapsulate diverse degrees of human-centered presupposed knowledge, including elements like form, dimension, hue, spatial orientations, concave and convex contours of shapes, and shape completion. Through

the employment of distinct querying approaches, the Bongard-logo and RPM tasks endeavor to evaluate the extractor’s expertise in unveiling and assimilating these abstract concepts.

This paper attempts to propose a methodology that relies on analyzing the distribution of images in the primary and auxiliary groups of Bongard-Logo problems to solve them. This methodology aims to provide a new direction different from the previous ones for solving Bongard-Logo problems.

A. A method for solving the bongard-logo problem based on sinkhorn distance (SBSD)

In the Bongard-Logo problem, we denote x_{ij} as the j -th image in the i -th Bongard-Logo problem, where $i \in [1, n]$ signifies the question number, with n being the total number of questions. Specifically, $\{x_{ij}\}_{j=1}^6$ represents images in the i -th primary group, while $\{x_{ij}\}_{j=8}^{13}$ represents images in the i -th auxiliary group. Additionally, x_{i7} represents the test image to be potentially assigned to the i -th primary group, and x_{i14} represents the test image to be potentially assigned to the i -th auxiliary group. We let the distribution of the primary group (positive examples) within a Bongard-Logo question be denoted as $p_i(x|y)$, and the distribution of the auxiliary group (negative examples) be denoted as $q_i(x|y)$. Here, y represents the reasoning type condition of the question, where $y \in \{ff, ba, hd\}$. We are committed to developing a deep learning algorithm that can induce distributions $p_i(x|y)$ and $q_i(x|y)$ with low cross-measure between them.

Therefore, we aim to devise a deep learning algorithm, denoted as $f_\theta(z|x)$, which can map samples x_{ij} to latent variables z_{ij} . We hope that $f_\theta(z|x)$ can serve as a distribution transformation function, and by measuring the distribution of the latent representation, we can address the Bongard-Logo problem. Thus, the key objective is to ensure that the cross-measure between the latent variable distribution of the primary group, denoted as $p'_i(z|y)$, and the latent variable distribution of the auxiliary group, denoted as $q'_i(z|y)$, is significantly low. The Kullback-Leibler (KL) divergence, a measure used to quantify the similarity between distributions, can be employed for this purpose [7]. The formula for calculating KL divergence is provided below.

$$KL(P||Q) = \sum P(x) \log \left(\frac{P(x)}{Q(x)} \right) \quad (1)$$

However, due to the characteristics of small sample learning problems, it is challenging to estimate the distributions $p'_i(z|y)$ and $q'_i(z|y)$ of Bongard-Logo image representations. Estimating the specific forms of distributions $p'_i(z|y)$ and $q'_i(z|y)$ poses an even greater challenge. Additionally, the limitations of the Kullback-Leibler (KL) divergence make it difficult to directly optimize for these conditions and obtain a highly effective deep model.

Hence, we endeavored to utilize baseline models, specifically ResNet18, for the purpose of encoding images within the Bongard-Logo paradigm, denoted as $\{x_{ij}\}_{j=1}^{14}$, into meaningful representations, designated as $\{z_{ij}\}_{j=1}^{14}$. These representations, in the context of a Bongard-Logo question, were interpreted as samples drawn from the distributions $p'_i(z|y)$

and $q'_i(z|y)$. Subsequently, constraints were imposed on the Sinkhorn distance between $p'_i(z|y)$ and $q'_i(z|y)$ through these representations. This methodology was designed primarily because the Sinkhorn algorithm computes the distance without requiring explicit knowledge of the distributions' specific forms, making it highly suitable for scenarios where the shapes of $p'_i(z|y)$ and $q'_i(z|y)$ remain unknown.

Specifically, the representations within the primary group, denoted as $\{z_{ij}\}_{j=1}^7$, were randomly partitioned into two distinct subgroups: $\{z_{it}\}$ and $\{z_{i\bar{t}}\}$. By utilizing the Sinkhorn distance between these subgroups, constraints were imposed to ensure that the representations within the primary group $\{z_{ij}\}_{j=1}^7$ adhered to a consistent, albeit unknown, distribution. Analogously, similar constraints were introduced between the distributions represented by $p'_i(z|y)$ and $q'_i(z|y)$, leveraging representations from both the primary and auxiliary groups to minimize the cross-measure.

The aforementioned constraints can be explicitly articulated through a mathematical loss function.

$$\begin{aligned} & \ell(\{z_{ij}\}_{j=1}^{14}) \\ &= -\log \frac{e^{-D(\{z_{it}\}, \{z_{i\bar{t}}\})}}{e^{-D(\{z_{it}\}, \{z_{i\bar{t}}\})} + e^{-D(\{z_{ij}\}_{j=1}^7, \{z_{ij}\}_{j=8}^{14})}} \end{aligned} \quad (2)$$

Let $D(a, b)$ denote the calculation of the Sinkhorn distance between the distributions associated with sets a and b . Additionally $\{z_{it}\} \cup \{z_{i\bar{t}}\} = \{z_{ij}\}_{j=1}^7$ and $\{z_{it}\} \cap \{z_{i\bar{t}}\} = \emptyset$. Despite our endeavors, this approach did not yield satisfactory results. We hypothesize that this was primarily due to the limited sample size within a single Bongard-logo problem, which, when collectively treated as sampling outcomes, may not meet the prerequisite sampling requirements of the Sinkhorn distance. An illustrative diagram depicting this process can be found in Figure 4.

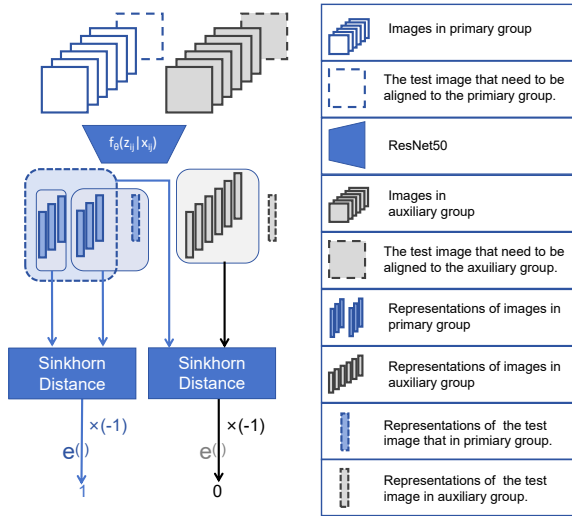


Fig. 4. Feedforward process of SBSD

In summary, SBSD treats the representations of images within the primary group as samples from the primary group distribution $p'_i(z|y)$, and the auxiliary group follows the same approach. By utilizing these samples, the Sinkhorn distance

is employed to constrain the distance between the primary $p'_i(z|y)$ and auxiliary distributions $q'_i(z|y)$.

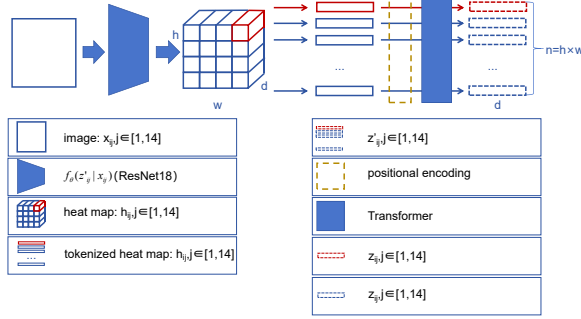
B. PMoC(Probability Model of Concept)

After conducting experiments, we discovered that SBSD had achieved limited progress in inference accuracy. However, this paper aims to make more contributions and breakthroughs. Therefore, by carrying forward the idea of analyzing primary and auxiliary group distributions in SBSD, this paper designs the deep model PMoC (Probability Model of Concept). PMoC explore an alternative approach by shifting the constraint conditions. The training objective has been shifted from focusing on the deep model's ability to disentangle distribution $p'_i(z|y)$ and distribution $q'_i(z|y)$ to emphasizing its capacity to compute the probability of a representation under the distribution $p'_i(z|y)$. For this purpose, we assume that $p'_i(z|y)$ follows a multivariate Gaussian distribution.

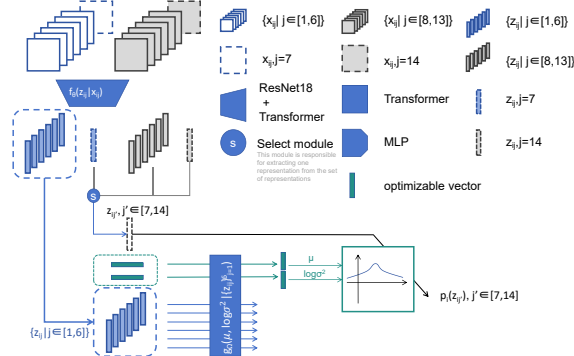
Our PMoC consists of two components: module $f_\theta(z|x)$ and module $g_\omega(\mu, \sigma^2|z)$. The module $f_\theta(z|x)$ maps the input x to its latent representation z , while $g_\omega(\mu, \sigma^2|z)$ is utilized to compute the μ and σ^2 for Gaussian distribution $p'_i(z|y)$.

In this paper, we define $\{x_{ij}\}_{j=1}^6$ as the primary group samples for the i -th Bongard-Logo question, with j denoting the sample number. Similarly, $\{x_{ij}\}_{j=8}^{13}$ represents the auxiliary group samples for the i -th question. x_{i7} and x_{i14} are the representations of the samples to be classified. Meanwhile, $\{z_{ij}\}_{j=1}^{14}$ represents the encoded Bongard-Logo samples $\{x_{ij}\}_{j=1}^{14}$, and the encoding process is implemented by $f_\theta(z_{ij}|x_{ij})$. Furthermore, we utilize a deep network, denoted as $g_\omega(\mu_i, \sigma_i|\{z_{ij}\}_{j=1}^6)$, to fit an optimizable multivariate Gaussian distribution $p'_i(z|\{z_{ij}\}_{j=1}^6, \omega)$, based on the primary group samples features $\{z_{ij}\}_{j=1}^6$. Subsequently, we calculate the probability of each representation in $\{z_{ij'}\}_{j'=7}^{14}$ belonging to this distribution, denoted as $\{p'_i(z_{ij'}|\{z_{ij}\}_{j=1}^6, \omega)\}_{j'=7}^{14}$. The network $f_\theta(z_{ij}|x_{ij})$ maps the input x_{ij} to its latent representation z_{ij} , while $g_\omega(\mu_i, \sigma_i|\{z_{ij}\}_{j=1}^6)$ is utilized to compute the distribution of the latent representations $\{z_{ij}\}_{j=1}^6$, and the distribution is modeled as Gaussian distribution. In other words, $f_\theta(\cdot)$ serves as an image encoder, and $g_\omega(\cdot)$ as a logical distribution fitter. Thus, we employ a Convolutional Neural Network (CNN) to fit $f_\theta(\cdot)$ and a Transformer-Encoder to fit $g_\omega(\cdot)$. Further design details are provided as follows.

We present an approach that combines ResNet18 with Transformer-Encoder, employing this integration as the architecture for the function $f_\theta(z_{ij}|x_{ij})$. In detail, we encode the Bongard-Logo problem images x_{ij} into feature maps $h_{ij} \in R^{h \times w \times d}$ using ResNet18. Subsequently, we calculate the self-attention results $z'_{ij} \in R^{n \times d}$ among all receptive fields within the feature maps h_{ij} . This computation enables the n attention outputs z'_{ij} to capture global information of the image in varying degrees, ensuring that each output retains some level of contextual understanding. We encoded Bongard-Logo images from multiple perspectives using the aforementioned method. We denote each individual perspective within z'_{ij} as $z_{ij} \in R^d$. The feedforward process of the network $f_\theta(z_{ij}|x_{ij})$ is illustrated in the figure 5.


 Fig. 5. Feedforward process of $f_\theta(z_{ij}|x_{ij})$

The network $g_\omega(\mu_i, \sigma_i | \{z_{ij}\}_{j=1}^6)$ is much more of its name. It encodes the mean and variance of the i -th primary group distribution based on the latent representations of the i -th primary group samples, and i still represents the problem index in Bongard-Logo. Specifically, we uniformly process each perspective z_{ij} within z'_{ij} . Under a single perspective, we treat $\{z_{ij}\}_{j=1}^6$ as six tokens and, after appending two optimizable vectors along with positional embedding, input them into $g_\omega(\mu_i, \sigma_i | \{z_{ij}\}_{j=1}^6)$ with a Transformer-Encoder backbone for computing attention results. We extract two optimizable vectors from the attention results, serving as the mean $\mu_i \in R^d$ and logarithm of variance $\log(\sigma_i^2) \in R^d$ for a multivariate Gaussian distribution. The encoding distribution pattern of module $g_\omega(\mu_i, \sigma_i | \{z_{ij}\}_{j=1}^6)$ follows a similar approach to that of VAE [7]; however, it does not incorporate variational inference in its design. The aforementioned process parameterizes $p'_i(z|y)$ as a multivariate Gaussian distribution and outlines the computation of $g_\omega(\mu_i, \sigma_i | \{z_{ij}\}_{j=1}^6)$. We feed 8 vectors $\{z_{ij'}\}_{j'=7}^{14}$ into this distribution for calculating 8 logical probabilities $\{p'_i(z_{ij'} | \{z_{ij}\}_{j=1}^6, \omega)\}_{j'=7}^{14}$ in one perspective. In this paper, we calculate the final probability $p'_i(z'_{i7})$ by averaging the logical probabilities $p'_i(z_{ij'} | \{z_{ij}\}_{j=1}^6, \omega)$ obtained from all perspectives. By utilizing the cross entropy loss function, we constrain the final probability $p'_i(z'_{i7})$ to approach 1 while ensuring other probabilities $\{p'_i(z'_{ij'})\}_{j'=8}^{14}$ are close to 0. Figure 6 illustrates in detail the forward process of the network $g_\omega(\mu_i, \sigma_i | \{z_{ij}\}_{j=1}^6)$ under a single perspective in $z_{ij} \in R^{n \times d}$. However, this approach did not yield satisfactory results.

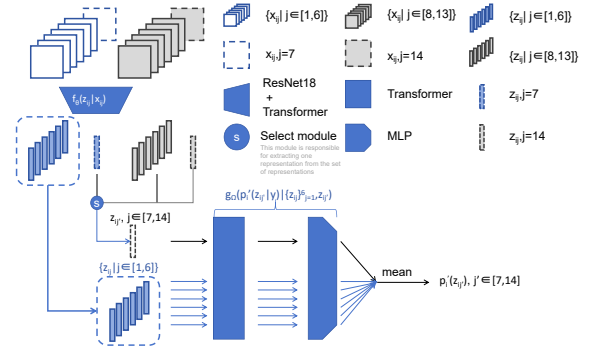

 Fig. 6. Feedforward process of $g_\omega(\mu_i, \sigma_i | \{z_{ij}\}_{j=1}^6)$.

We speculate that the reason for the ineffectiveness of the aforementioned method lies in the unknown true form of the distribution $p'_i(z|y)$, which may be a complex mixed Gaussian distribution. Therefore, it may not be reasonable to parameterize $p'_i(z|y)$ as a multivariate Gaussian distribution and compute the probability $p'_i(z_{ij'}|y)$. Additionally, the formula for calculating the logical probability of a vector z belonging to the parameterized distribution is provided as follows.

$$\log(p(z, \mu, \sigma)) = \frac{(z_m - \mu_m)^2}{2\sigma_m^2} - \log(|\sigma_m|) - \frac{1}{2} \log(2\pi) \quad (3)$$

Where m represents the dimension index of the vector. μ represents the mean of the multivariate Gaussian distribution, σ represents the standard deviation of the multivariate Gaussian distribution, and z is the representation of some unknown data. It is evident that optimizing the network using the given formula (3) as the loss function presents challenges, as optimizing the above equation can be indirectly viewed as optimizing the Mean Squared Error (MSE) loss between vectors. Moreover, these vectors have not undergone normalization or squashing, making it difficult to optimize the network from the perspective of implementation. Consequently, in this paper, we train a deep network to directly fit probability $p'_i(z_{ij'}|y)$. Inevitably the network's formulation has been transformed from $g_\omega(\mu_i, \sigma_i | \{z_{ij}\}_{j=1}^6)$ to $g_\omega(p'_i(z_{ij'}|y) | \{z_{ij}\}_{j=1}^6, z_{ij'})$, thereby simplifying the problem.

Different from previous approaches $g_\omega(\mu_i, \sigma_i | \{z_{ij}\}_{j=1}^6)$ that fit the distribution $p'_i(z|y)$, this paper employs a Transformer-Encoder to fit the probability $p'_i(z_{ij'}|y)$ directly, which enables the direct computation of the probability that $z_{ij'}$ belongs to the distribution $p'_i(z|y)$.


 Fig. 7. Feedforward process of $g_\omega(p'_i(z_{ij'}|y) | \{z_{ij}\}_{j=1}^6, z_{ij'})$.

Specifically, in this paper, we maintain an egalitarian approach towards each perspective $z_{ij} \in R^d$ within the outcomes $z'_{ij} \in R^{n \times d}$ of $f_\theta(z_{ij}|x_{ij})$. Within the confines of a singular perspective, we amalgamate $\{z_{ij}\}_{j=1}^6$ with one of the pending representations $\{z_{ij'}\}_{j'=7}^{14}$, resulting in a set of seven tokens. Following the embedding of positional encoding, these tokens are then systematically fed into a Transformer-Encoder, aimed at yielding 7 attention results. All 7 attention results are mapped to 7 probabilities by a MLP. The mean of the mapped outcomes is considered as the logical probability $p'_i(z_{ij'}|y)$

corresponding to the specified perspective. This constitutes the feedforward process of the new $g_\omega(p'_i(z_{ij'}|y)|\{z_{ij}\}_{j=1}^6, z_{ij'})$. Each pending representation $z_{ij'}$, receives a corresponding probability output $p'_i(z_{ij'}|y)$. Each logical probabilities $\{p'_i(z_{ij'}|y)\}_{j'=7}^{14}$ are averaged to yield the final probability value $\{p'_i(z_{ij'}|y)\}_{j'=7}^{14}$. In this paper, we still optimize the model using the cross-entropy loss function. Figure 7 visually depicts the process of $g_\omega(p'_i(z_{ij'}|y)|\{z_{ij}\}_{j=1}^6, z_{ij'})$ handling a single perspective.

In summary, this paper makes two compromises for PMoC. Firstly, we acknowledge that compared to $p'_i(z)$, $q'_i(z)$ is more likely to be a complex distribution. For instance, $p'_i(z)$ may follow a Gaussian distribution, while $q'_i(z)$ may adhere to a mixed Gaussian distribution. Consequently, we shift our focus to estimating the distribution $p'_i(z)$ and utilize the probability of a representation belonging to this distribution to determine whether it is a primary or auxiliary group representation. Secondly, due to the challenges associated with optimizing the model from the perspective of estimating $p'_i(z)$, this paper opts to directly compute the probability of a representation belonging to the distribution $p'_i(z)$.

IV. METHODOLOGY FOR ABSTRACT REASONING

Previous research has demonstrated limited success in learning abstract concepts related to positional relationships among entities, particularly when addressing the Bongard-Logo and RPM problems. This limitation is evident in challenges posed by the OIG and D-9 problem sets from RAVEN, as well as the ff and hd issues of Bongard-Logo and the Neurtal problem in PGM. The RS-model [31], however, overcame these difficulties by explicitly incorporating additional structural cues (meta data, auxiliary label), achieving commendable inferential accuracy.

In this section, we introduce the Pose-Transformer, an enhancement to the Transformer-Encoder framework that incorporates the pose matrix from the Capsule Network [33]. This integration implicitly enhances the network’s ability to discern positional relationships among local representations, thereby bolstering its learning capabilities on graphical abstract reasoning problem. Furthermore, we have lightweighted Pose-Transformer into Straw-Pose Transformer, which achieves a lightweight version of the former while maintaining its effectiveness. We present and delve into the intricacies of our proposed Pose-Transformer, discussing its potential to revolutionize learning in tasks that involve complex positional relationships through experiments.

A. Pose-transformer

We delve into the intricacies of the Transformer-Encoder framework, particularly when it processes logical inputs to generate attention-weighted outputs. During this process, all output tokens become associated with varying degrees of global information derived from the logical inputs [27], [34]. Operating on a multi-head self-attention mechanism, the Transformer-Encoder segments the input tokens into multiple sub-vectors and computes their self-attention results in parallel [34]. From an informational standpoint, we postulate that these

segmented sub-vectors possess lesser information compared to the holistic tokens encoding global information, effectively rendering them as representations of localized information. Consequently, the relative positional relationships among these localized informational units warrant a summarization and analysis.

Specifically, we have designed a novel fundamental module termed “pose matrix embedding” tailored for the RPM and Bongard-Logo problems. When logical inputs $\{\tilde{V}_i|i \in [1, n], \tilde{V}_i \in R^d\}$ pass through a single Transformer-Encoder layer, this paper segments the n output tokens $\{V_i|i \in [1, n], V_i \in R^d\}$, attention results, into m local vectors $\{H_{ij}|i \in [1, n], j \in [1, m], H_{ij} \in R^{d/m}\}$ of the attention head size. A set of mapping matrices $\{W_{ijk}|i \in [1, n], j \in [1, m], k \in [1, n], W_{ijk} \in R^{(d/m) \times d}\}$ is established for each local vector, with the number of matrices k within a set being identical to the token count n of the logical input. These mapping matrices facilitate the transformation of local vectors into pose vectors $(H_{ij} \times W_{ijk})$. We compute the entire set of pose vectors $\{P_{ijk}|i \in [1, n], j \in [1, m], k \in [1, n], P_{ijk} \in R^d\}$ resulting from the mapping of each local vector. By summing and squashing these pose vectors and adding them to $\{V_i|i \in [1, n], V_i \in R^d\}$, we obtain the logical output $\{O_k|k \in [1, n], O_k \in R^d\}$ of the foundational block of pose-transformer. The squashing function is formulated as shown in the equation below:

$$\text{squash}(\mathbf{v}) = \frac{\|\mathbf{v}\|^2}{1 + \|\mathbf{v}\|^2} \cdot \frac{\mathbf{v}}{\|\mathbf{v}\|} \quad (4)$$

where the operator $\|\cdot\|$ is L_2 norm. It is worth mentioning that the squash function, $\text{squash}(\cdot)$, is employed in Capsule Networks to squash pose vectors for computing pose consistency among all local representations. Similarly, in the context of pose-transformer, the squash function continues to serve its purpose and retain its significance, contributing to the overall architecture’s efficacy. The feedforward process of a single pose matrix embedding fundamental block is illustrated in the figure 8. The entire calculation process of “pose matrix embedding” can be expressed as follows:

$$\{V_i|i \in [1, n]\} = \text{T-Encoder}(\{\tilde{V}_i|i \in [1, n]\}) \quad (5)$$

$$\{H_{ij}|j \in [1, m]\} = \text{segment}(V_i) \quad (6)$$

$$P_{ijk} = H_{ij} \times W_{ijk} \quad (7)$$

$$O_k = (V_i|i = k) + \text{squash}\left(\sum_{i=1}^n \sum_{j=1}^m P_{ijk}\right) \quad (8)$$

In the formula, the term “segment” represents the aforementioned cutting process. The process of feeding the input vector set into the transformer-encoder to obtain the output is denoted as “T-Encoder”.

This fundamental block is followed by a feedforward block, forming the basic building block of the Pose-Transformer. The design of the feedforward block is consistent with that in the Transformer-Encoder architecture. Notably, the proposed fundamental block is dimension-preserving, allowing for the stacking of multiple blocks to adapt to dif-

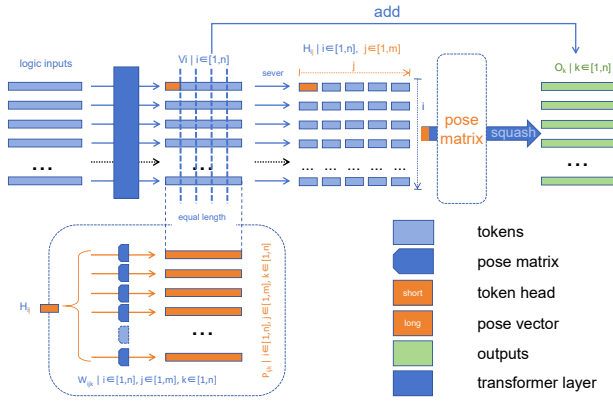


Fig. 8. The feedforward process of a single pose matrix embedding block

ferent scales of graphical reasoning problems. The Pose-Transformer with N logical layers is depicted in the figure 9. When $N = 1$, the Pose-Transformer collapses into a regular Transformer-Encoder. In Capsule Networks, similarity weights are distributed across higher-level capsules and computed in a bottom-up fashion, whereas attention weights in the Transformer-Encoder are distributed over lower-level representations and computed top-down. In the Pose-Transformer with $N > 1$, similarity weights for local representations can be calculated at multiple levels and scales from the outside in. This is ensured by the fact that each logical layer in the Pose-Transformer is succeeded by a standard Transformer-Encoder layer, which can be present in the subsequent logical layer or the terminating layer, responsible for recalculating the similarity weights.

The Pose-Transformer diverges from the dynamic routing mechanism of Capsule Networks, which iteratively computes representation similarity weights. Instead, it employs an attention mechanism to perform the task of the routing. For the complete computation of similarity weights, the Pose-Transformer terminates with a standard Transformer-Encoder layer, which serves as the final stage for calculating similarity weights on the pose vectors.

B. Straw Pose-transformer

Pose-Transformer, during deployment, exerts considerable pressure on computational resources. The establishment and computation of the mapping matrices, denoted as $\{W_{ijk} | i \in [1, n], j \in [1, m], k \in [1, n], W_{ijk} \in R^{(d/m) \times d}\}$, incur significant resource overhead. Motivated by this challenge, this paper explores the lightweighting of Pose-Transformer. The crux of Pose-Transformer lies in computing compressed pose vectors and subsequently employing them to modify and refine the logical inputs, represented as $\{V_i | i \in [1, n], V_i \in R^d\}$ to some extent. The computation of the logical outputs in Pose-Transformer's pose matrix mapping follows the methodology outlined below:

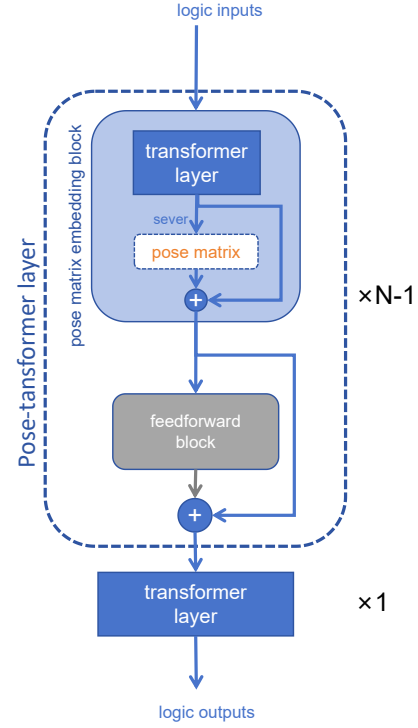


Fig. 9. The architecture of the pose-transformer

$$O_k = V_i + \text{squash} \left(\sum_i^n \sum_j^m H_{ij_} \times W_{ijk} \right) \quad (9)$$

It is worth noting that the placeholders marked with “_” in the formula represent numbering for on-demand broadcasting. Multiple levels of summation and mapping can incur significant computational overhead. By designing parameter sharing, we aim to eliminate partial logical summation and mapping, thereby achieving the purpose of reducing computational cost. From a logical hierarchy perspective, only the numbering at the i -th level has the potential for indentation, while other logical levels have strong mapping requirements. In other words, this paper posits that the pose matrices between equivalent local vectors across different tokens merit weight sharing. The planned target expression of pose matrix mapping after indentation is:

$$O_k = V_i + \text{squash} \left(\sum_i^n \sum_j^m H_{j_} \times W_{jk} \right) \quad (10)$$

This paper aims to simplify the Pose-Transformer based on the aforementioned expression. We treat the mapping matrix W_{ijk} as a product of the mapping matrix \tilde{W}_{jk} multiplied by i different coefficients, specifically expressed as $W_{ijk} \doteq w_i \cdot \tilde{W}_{jk}$. This transformation significantly reduces the number of matrices involved. We argue that it is more reasonable to combine w_i with $H_{ij_}$ and treat them as a weighted sum of $H_{ij_}$, rather than treating w_i as an optimizable weight

vector. Furthermore, treating this process as computing an attention-weighted sum for H_{ij_-} is even more elegant and effective. Therefore, we propose a feasible solution that involves embedding a learnable vector V_0 , where $V_0 \in R^d$ and we denote $\{H_{0j}|j \in [1, m], H_{0j} \in R^{(d/m)}\}$ as the attention heads corresponding to V_0 , and computing the multi-head cross-attention results between V_0 and $\{V_i|i \in [1, n]\}$. This approach aligns well with the formula presented:

$$O_k = V_i + \text{squash} \left(\sum_i^n \sum_j^m H_{ij_-} \times W_{ijk} \right) \quad (11)$$

$$\begin{aligned} \tilde{O}_k &= V_i + \text{squash} \left(\sum_i^n \sum_j^m H_{ij_-} \times (w_i \cdot \tilde{W}_{jk}) \right) \\ &= V_i + \text{squash} \left(\sum_j^m \left(\sum_i^n w_i \cdot H_{ij_-} \right) \times \tilde{W}_{jk} \right) \\ &= V_i + \text{squash} \left(\sum_j^m \tilde{H}_{j_-} \times \tilde{W}_{jk} \right) \\ &= V_i + \text{squash} \left(\sum_j^m \tilde{H}_{j_-} \times \tilde{W}_{jk} \right) \\ &\doteq V_i + \text{squash} \left(\sum_j^m \text{Attention}(H_{ij_-}) \times \tilde{W}_{jk} \right) \quad (12) \end{aligned}$$

Notably, the aforementioned approach necessitates computing cross-attention additionally between the standard Transformer-Encoder layer and pose mapping, which prolongs the training time, contradicting the intended purpose. This paper utilizes a transformer encoder with an additional mask mechanism to integrate the transformer encoding process with the multi-head cross attention computation process.

Specifically, this paper introduces an optimizable vector, denoted as $\tilde{V}_0 \in R^d$, for the embedding of logical inputs $\{\tilde{V}_i|i \in [1, n], V_i \in R^d\}$. This vector is akin to the class learning vector in the Vision Transformer (ViT). After the logical inputs, augmented with a learnable vector \tilde{V}_0 , propagate through a single Transformer-Encoder layer while applying a mask to the self-attention weights at the position corresponding to \tilde{V}_0 to prevent its value mapping from contributing to the attention results of the Transformer-Encoder, they produce an updated set of vectors $\{V_i|i \in [0, n], V_i \in R^d\}$ representing the attention-weighted outputs. Our aim is to accomplish two processes within a single self-attention computation: the extra multi-head cross-attention between \tilde{V}_0 and $\{\tilde{V}_i|i \in [1, n]\}$, and the pre-existing multi-head self-attention among $\{\tilde{V}_i|i \in [1, n]\}$. We replace the tedious sequential process with this masked attention mechanism, thereby streamlining the computational workflow. Due to the inherent self-attention mechanism and masking, the vector \tilde{V}_0 assimilates information from the logical inputs, transforming into global vector V_0 . Within this global vector, we establish a collection of mapping matrices $\{W_{jk}|j \in [1, m], k \in [1, n], W_{jk} \in R^{(d/m) \times d}\}$ for each attention head $\{H_{0j}|j \in [1, m], H_{0j} \in R^{(d/m)}\}$ in it.

It is evident that there exists a subtle difference between the masked attention process and the sequential process of self-attention and cross-attention, which renders them not strictly equivalent. Conversely, the masked attention process is equivalent to a serial process of performing cross-attention followed by self-attention. However, ignoring the sequence and merging the two processes of attention-based weighted summation into one step is not an unreasonable approach. In fact, this merger can be seen as a computational optimization that reduces the amount of computation and improves efficiency.

The pose vectors $\{p_{jk}|j \in [1, m], k \in [1, n], p_{jk} \in R^d\}$ is achieved by multiplying the attention heads with the mapping matrices. These pose vectors, after summation and squashing, are added to the vector set $\{V_i|i \in [1, n], V_i \in R^d\}$ to obtain the output of new pose matrix mapping block $\{O_i|i \in [1, n], O_i \in R^d\}$. This process outlines the computation process of the pose embedding matrix block within the Straw Pose-Transformer architecture. The entire calculation process of new ‘‘pose matrix embedding’’ can be expressed as follows:

$$\{V_i|i \in [0, n]\} = \text{Masked T-Encoder}(\{\tilde{V}_i|i \in [0, n]\}) \quad (13)$$

$$\{H_{0j}|j \in [1, m]\} = \text{segment}(V_0) \quad (14)$$

$$P_{jk} = H_{0j} \times \tilde{W}_{jk} \quad (15)$$

$$O_k = (V_i|i = k) + \text{squash} \left(\sum_{j=1}^m P_{jk} \right) \quad (16)$$

In the formula, the process of the Masked transformer-encoder to obtain the output is denoted as ‘‘Masked T-Encoder’’. In the Straw Pose-Transformer architecture, the outputs from each logical layer, denoted as $\{O_k|k \in [1, n]\}$, undergo a concatenation process with the global vector V_0 attached to their precursors. This modified set, now represented as $\{\tilde{V}_i|i \in [0, n]\}$, is then propagated into the subsequent logical layer for further processing. However, if the subsequent logical layer is the final layer, the global vector V_0 is no longer appended.

In this way, we can reconstruct the pose matrix embedding process according to the formula, and this feedforward process is illustrated in the figure 10. It is worth mentioning that masking the position corresponding to V_0 in the attention coefficients reduces the impact of the optimizable parameter V_0 on the pose mapping process to a certain extent, making it a relatively necessary operation. our analysis demonstrates that this stabilizes training and improves inference accuracy somewhat. This paper replaces the standard Transformer-Encoder+cross-attention+pose matrix mapping sequential process in pose-Transformer with the aforementioned procedure. And figure 11 illustrate the structure of the Straw-Pose-Transformer.

In summary, our lightweighting strategy for Pose-Transformer involves the insertion of additional cross-attention computations between the original Transformer-Encoder calculations and the pose matrix mapping computations. While this approach reduces the number of parameters, it also elongates the training time, which is an undesirable trade-off. Therefore, in this study, we have designed a masked

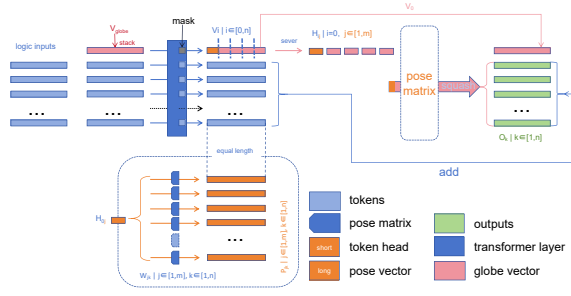


Fig. 10. The feedforward process of a single Straw pose matrix embedding block

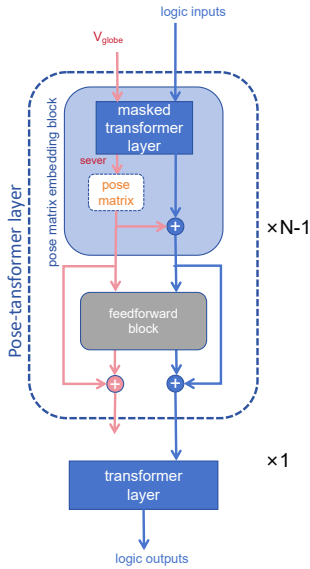


Fig. 11. The architecture of the straw pose-Transformer

Transformer-Encoder that obviates the need for explicitly inserting cross-attention computation processes, aiming to achieve a more efficient and streamlined model.

V. COMBINATION OF POSE-TRANSFORMER AND BASELINES

In addressing the Bongard-Logo problem, this paper introduces a novel baseline, PMoC. To demonstrate the adaptability of the Straw-Pose-Transformer in solving the Bongard-Logo problem, the Transformer-Encoder component within PMoC is replaced with the Straw-Pose-Transformer in this section. Furthermore, given the remarkable performance achieved by the predecessor RS-Tran in solving the RPM problem, this paper does not design an additional baseline network to prove the superiority of the Pose-Transformer in addressing the RPM problem. This paper aims to demonstrate the advantage of Pose-Transformer over the standard Transformer-Encoder for RPM problems by achieving improved accuracy through the simple replacement of the Transformer-Encoder in RS-Tran with Pose-Transformer.

The RS-Tran [31] primarily consists of Transformer-Encoder structures, and in this study, we replace it with the Pose-Transformer and Straw-Pose-Transformer and conduct experiments. The modified RS-Tran is renamed as RS-Pose-Tran and RS-Straw-Pose-Tran. Due to the fundamental modifications made to the RS-Tran architecture, RS-Pose-Tran and RS-Straw-Pose-Tran can be regarded as models designed based on our novel structure, incorporating inductive biases inherent in the RPM problem [37]. Subsequently, it was discovered that compared to the Transformer-Encoder, the Pose-Transformer exhibits greater suitability for abstract reasoning problems, specifically the RPM and Bongard-Logo problems.

VI. EXPERIMENT

In this section, we conduct experiments on the model proposed in this paper.

A. Experiment on Bongard-Logo

We conducted experiments on the Bongard-logo dataset using the SBSD and PMoC model. The results are recorded in Table I. Due to the serial convolution scanning mechanism and attention mechanism being prone to attention collapse, the parameters of the SBDC model are utilized as pre-trained parameters for the PMoC convolutional layer. In addition, this study experimented with the combination of the Straw pose-transformer and PMoC. It is worth noting that, under the experimental conditions of this paper, which involved four A100s graphics processing units (GPUs), the integration of PMoC with the pose-transformer proved to be challenging to deploy. This is one of the reasons and motivations behind our decision to design a lightweight approach for Pose-Transformer in this paper.

All our experiments are implemented in Python using the PyTorch [38] framework. In the experiments conducted for PMoC and SBSD, the Adam [39] optimizer was selected with a learning rate set to 0.001, a learning rate decay of 0.995, a weight decay of 0.0001, and a batch size of 40 for PMoC and SBSD. Specifically, in the experiment combining PMoC with straw-pose-transformer, the batch size was set to 20.

In Table I, it is evident that addressing the Bongard-Logo problem using a probabilistic model approach, namely PMoC, is both straightforward and effective. Furthermore, SBSD exhibits stronger outcomes when compared to previous models. Additionally, the integration of Straw-Pose-Transformer has contributed significantly to enhancing the inference accuracy of PMoC.

B. Experiment on RPM

We conducted experiments on I-RAVEN and PGM by sequentially replacing the Transformer structure in RS-Tran with Pose-Transformer and Straw-Pose-Transformer. The results of I-RAVEN are recorded in Table II and PGM is recorded in Table III. In this paper, we considered that compared to the standard Transformer-Encoder, a single layer of Pose-Transformer and its lightweight version possess twice the

TABLE I
REASONING ACCURACIES OF DC ON BONGARD-LOGO.

Model	Accuracy(%)				
	Train	FF	BA	CM	NV
SNAIL	59.2	56.3	60.2	60.1	61.3
ProtoNet	73.3	64.6	72.4	62.4	65.4
MetaOptNet	75.9	60.3	71.6	65.9	67.5
ANIL	69.7	56.6	59.0	59.6	61.0
Meta-Baseline-SC	75.4	66.3	73.3	63.5	63.9
Meta-Baseline-MoCo	81.2	65.9	72.2	63.9	64.7
WReN-Bongard	78.7	50.1	50.9	53.8	54.3
SBSD	83.7	75.2	91.5	71.0	74.1
PMoC	92.0	92.6	97.7	78.3	75.0
PMoC+Straw Pose-Transformer	96.2	96.0	98.5	78.5	75.3

number of logical computations. Therefore, the combined RS-Pose-Tran and RS-Straw-Pose-Tran only stacked half of the logical layers of RS-Tran to ensure that the internal logical computation times of the three models were equivalent. In addition, the parameter settings and dataset configurations for the experiments related to RS-Pose-Tran were strictly maintained consistent with those of RS-Tran. Such a setting renders the comparative results of the three models more convincing.

TABLE II
REASONING ACCURACIES ON RAVEN AND I-RAVEN.

Model	Test Accuracy(%)							
	Average	Center	2 × 2 Grid	3 × 3 Grid	L-R	U-D	O-IC	O-IG
SAVIR-T [27]	94.098.1	97.899.5	94.798.1	83.893.8	97.899.6	98.299.1	97.699.5	88.097.2
SCL [26], [27]	91.695.0	98.199.0	91.096.2	82.589.5	96.897.9	96.597.1	96.097.6	80.187.7
MRNet [21]	96.6/-	-/-	-/-	-/-	-/-	-/-	-/-	-/-
RS-TRAN [31]	98.498.7	99.8/100.0	99.799.3	95.496.7	99.2/100.0	99.499.7	99.9/99.9	95.495.4
RS-Pose-TRAN	-99.51	-100.00	-99.90	-98.20	-100.00	-100.00	-99.94	-98.56
RS-Straw-Pose-TRAN	-99.44	-100.00	-99.81	-98.12	-100.00	-100.00	-99.97	-98.22

In Table III, it can be seen that we did not conduct experiments on RS-Pose-Tran for PGM. This is because compared to RS-Tran operating on the RAVEN dataset, the overall dimension of the RS-Tran model doubles on PGM. However, such a doubling is prohibitive for RS-Pose-Tran, making it undeployable on our equipment and device. This motivated us to lightweight the Pose-Transformer into the Straw-Pose-Transformer in this paper.

TABLE III
REASONING ACCURACIES ON PGM.

Model	Test Accuracy(%)
SAVIR-T [27]	91.2
SCL [26], [27]	88.9
MRNet [21]	94.5
RS-CNN [31]	82.8
RS-TRAN [31]	97.5
RS-Straw-Pose-TRAN	98.64

From the perspective of experimental results, it is not

difficult to find that our lightweight approach has been successful without significantly reducing the performance of RS-Pose-Tran. Furthermore, the introduction of the pose mapping matrix into the Transformer-Encoder is effective, significantly improving the performance of RS-Tran. This demonstrates that Pose-Transformer is more suitable for abstract reasoning capabilities compared to the standard Transformer-Encoder, even though the standard Transformer-Encoder structure has shown strong advantages in RPM and Bongard-logo problems.

VII. CONCLUSION

In this paper, we presented an empirical study on the Bongard-logo dataset using the PMoC model and conducted experiments on I-RAVEN and PGM by replacing the Transformer structure in RS-Tran with Pose-Transformer and Straw-Pose-Transformer, sequentially.

Our experimental results demonstrate that PMoC has achieved competitive results on the Bongard-logo problem, successfully tackling it in the form of a probabilistic model. The two compromises made in the model design for implementing the PMoC are effective and reasonable. And the results also show that the introduction of the pose mapping matrix into the Transformer-Encoder is effective, achieving a significant breakthrough in the already remarkable accuracy of RS-Tran. These results suggest that Pose-Transformer is more advantageous for abstract reasoning tasks compared to the standard Transformer-Encoder, even though the latter has exhibited strong capabilities in RPM and Bongard-logo problems. Furthermore, our lightweight approach has been successful without significantly reducing the performance of RS-Pose-Tran.

In conclusion, our study highlights the effectiveness of incorporating pose mapping matrix into Transformer-Encoder for improving abstract reasoning capabilities. The successful implementation of our lightweight approach without significant performance reduction further strengthens the potential of Pose-Transformer in addressing complex reasoning tasks. The ingenious design of PMoC avoids to directly constrain the distribution of the latent representation of Bongard-Logo images, as well as the rigid modeling of this distribution into a known form. Experimental results demonstrate that such a design choice in PMoC is highly reasonable and effective. Furthermore, Pose-Transformer, leveraging PMoC, has exhibited its superiority in addressing the Bongard-logo problem.

REFERENCES

- [1] Deng, J., Dong, W., Socher, R., Li, L. J., Li, K., & Fei-Fei, L. Imagenet: A large-scale hierarchical image database. In IEEE Conference on Computer Vision and Pattern Recognition, 246-255 (2009).
- [2] He, K., Zhang, X., Ren, S., & Sun, J. Deep Residual Learning for Image Recognition. In IEEE Conference on Computer Vision and Pattern Recognition, 770-778 (2016).
- [3] Krizhevsky, A., Sutskever, I., & Hinton, G. E. Imagenet classification with deep convolutional neural networks. Communications of the ACM, 60(6), 84-90 (2017).
- [4] Vaswani, A. *et al.* Attention is All You Need. In Advances in Neural Information Processing Systems, (2017).
- [5] Devlin, J., Chang, M. W., Lee, K., & Toutanova, K. Bert: Pre-training of Deep Bidirectional Transformers for Language Understanding. Preprint at <https://arxiv.org/abs/1810.04805> (2018).

- [6] Brown, T. *et al.* Language Models are Few-shot Learners. In *Advances in Neural Information Processing Systems*, 1877-1901 (2020).
- [7] Kingma, D. P., & Welling, M. Auto-encoding variational bayes. Preprint at <https://arxiv.org/abs/1312.6114> (2014).
- [8] Goodfellow, I. *et al.* Generative adversarial networks. *Communications of the ACM*, 63(11), 139-144 (2020).
- [9] Ho, J., Jain, A., & Abbeel, P. Denoising diffusion probabilistic models. In *Advances in Neural Information Processing Systems*, 33, 6840-6851 (2020).
- [10] Antol, S., Agrawal, A., Lu, J., Mitchell, M., Batra, D., Zitnick, C. L., & Parikh, D. VQA: Visual question answering. In *IEEE International Conference on Computer Vision*, 2425-2433 (2015).
- [11] Johnson, J., Hariharan, B., Van Der Maaten, L., Fei-Fei, L., Lawrence Zitnick, C., & Girshick, R. Girshick. CLEVR: A Diagnostic Dataset for Compositional Language and Elementary Visual Reasoning. In *IEEE Conference on Computer Vision and Pattern Recognition*, 2901-2910 (2017).
- [12] Wang, X., Wei, J., Schuurmans, D., Le, Q., Chi, E., & Zhou, D. Self-Consistency Improves Chain of Thought Reasoning in Language Models. Preprint at <https://arxiv.org/abs/2203.11171> (2022).
- [13] Drori, I. *et al.* A Neural Network Solves, Explains, and Generates University Math Problems by Program Synthesis and Few-shot Learning at Human Level. *Proceedings of the National Academy of Sciences*, 119 (2022).
- [14] Chen, M. *et al.* Evaluating Large Language Models Trained on Code. Preprint at <https://arxiv.org/abs/2107.03374> (2021).
- [15] Raven J. C. Raven's Progressive Matrices. (Western Psychological Services, (1938).
- [16] Depeweg, S., Rothkopf, C. A., & Jäkel, F. Solving Bongard Problems with a Visual Language and Pragmatic Reasoning. Preprint at <https://arxiv.org/abs/1804.04452> (2018).
- [17] Nie, W., Yu, Z., Mao, L., Patel, A. B., Zhu, Y., & Anandkumar, A. Bongard-LOGO: A New Benchmark for Human-Level Concept Learning and Reasoning. In *Advances in Neural Information Processing Systems*, 16468-16480 (2020).
- [18] Zhang, C., Gao, F., Jia, B., Zhu, Y., & Zhu, S. C. Raven: A Dataset for Relational and Analogical Visual Reasoning. In *Proceedings of the IEEE/CVF Conference on Computer Vision and Pattern Recognition*, 5317-5327 (2019).
- [19] Barrett, D., Hill, F., Santoro, A., Morcos, A., & Lillicrap, T. Measuring Abstract Reasoning in Neural Networks. In *International Conference on Machine Learning*, 511-520 (2018).
- [20] Hu, S., Ma, Y., Liu, X., Wei, Y., & Bai, S. Stratified Rule-Aware Network for Abstract Visual Reasoning. In *Proceedings of the AAAI Conference on Artificial Intelligence*, 1567-1574 (2021).
- [21] Benny, Y., Pekar, N., & Wolf, L. Scale-Localized Abstract Reasoning. In *Proceedings of the IEEE/CVF Conference on Computer Vision and Pattern Recognition*, 12557-12565, (2021).
- [22] Zhang, C., Jia, B., Gao, F., Zhu, Y., Lu, H., & Zhu, S. C. Learning Perceptual Inference by Contrasting. In *Proceedings of Advances in Neural Information Processing Systems*, (2019).
- [23] Zheng, K., Zha, Z. J., & Wei, W. Abstract Reasoning with Distracting Features. In *Advances in Neural Information Processing Systems*, (2019).
- [24] Zhuo, T., & Kankanhalli, M. Effective Abstract Reasoning with Dual-Contrast Network. In *Proceedings of International Conference on Learning Representations*, (2020).
- [25] Zhuo, Tao and Huang, Qiang & Kankanhalli, Mohan. Unsupervised abstract reasoning for raven's problem matrices. *IEEE Transactions on Image Processing*, 8332-8341, (2021).
- [26] Wu, Y., Dong, H., Grosse, R., & Ba, J. The Scattering Compositional Learner: Discovering Objects, Attributes, Relationships in Analogical Reasoning. Preprint at <https://arxiv.org/abs/2007.04212> (2020).
- [27] Sahu, P., Basioti, K., & Pavlovic, V. SAViR-T: Spatially Attentive Visual Reasoning with Transformers. Preprint at <https://arxiv.org/abs/2206.09265> (2022).
- [28] Zhang, C., Jia, B., Zhu, S. C., & Zhu, Y. Abstract Spatial-Temporal Reasoning via Probabilistic Abduction and Execution. In *Proceedings of the IEEE/CVF Conference on Computer Vision and Pattern Recognition*, 9736-9746 (2021).
- [29] Zhang, C., Xie, S., Jia, B., Wu, Y. N., Zhu, S. C., & Zhu, Y. Learning Algebraic Representation for Systematic Generalization. In *Proceedings of the European Conference on Computer Vision*, (2022).
- [30] Hersche, M., Zeqiri, M., Benini, L., Sebastian, A., & Rahimi, A. A Neuro-vector-symbolic Architecture for Solving Raven's Progressive Matrices. Preprint at <https://arxiv.org/abs/2203.04571> (2022).
- [31] Q. Wei, D. Chen, B. Yuan, Multi-viewpoint and multi-evaluation with felicitous inductive bias boost machine abstract reasoning ability, arXiv :2210.14914, 2022.
- [32] S.Kharagorgiev, "Solving bongard problems with deep learning," k10v.github.io, 2020.
- [33] Sabour, Sara, Nicholas Frosst, and Geoffrey E. Hinton. "Dynamic routing between capsules." *Advances in neural information processing systems* 30 (2017).
- [34] Dosovitskiy, A. *et al.* An Image is Worth 16x16 Words: Transformers for Image Recognition at Scale. Preprint at <https://arxiv.org/abs/2010.11929> (2020).
- [35] Cuturi, Marco. "Sinkhorn distances: Lightspeed computation of optimal transport." *Advances in neural information processing systems* 26 (2013).
- [36] Shen, Jian, et al. "Wasserstein distance guided representation learning for domain adaptation." *Proceedings of the AAAI Conference on Artificial Intelligence*. Vol. 32. No. 1. 2018.
- [37] Carpenter, P. A., Just, M. A., & Shell, P. What One Intelligence Test Measures: a Theoretical Account of the Processing in the Raven Progressive Matrices Test. *Psychological review*, 97(3), 404, (1990).
- [38] Paszke, A. *et al.* Automatic Differentiation in Pytorch. In *NIPS Autodiff Workshop*, (2017).
- [39] Kingma, D. P., & Ba, J. Adam: A Method for Stochastic Optimization. Preprint at <https://arxiv.org/abs/1412.6980>, (2014).